crystals

MDPI

Article

The Universal Scaling of Dielectric Response as a Tool in the Description of a Complex Dynamic of 4′-Butyl-4-(2-methylbutoxy)azoxybenzene (4ABO5*)

Marcin Piwowarczyk, Ewa Juszyńska-Gałązka and Mirosław Gałązka *

Institute of Nuclear Physics Polish Academy of Sciences, ul. E. Radzikowskiego 152, 31-342 Kraków, Poland; marcin.piwowarczyk@ifj.edu.pl (M.P.); ewa.juszynska-galazka@ifj.edu.pl (E.J.-G.)
* Correspondence: miroslaw.galazka@ifj.edu.pl

Abstract: The results of dielectric relaxation spectroscopy of the chiral liquid crystal 4′-butyl-4-(2-methylbutoxy)azoxybenzene in the crystal phase are presented. The scaling procedure showed complex molecular dynamics and allows one to decompose the observed relaxation process into two closely located relaxation processes around the short molecular axis. Temperature dependences of relaxation times characterizing flip-flop motions (rotation around the short molecular axis) and rotation around the long molecular axis are of the Arrhenius type.

Keywords: liquid crystal; dielectric spectroscopy; molecular relaxation; scaling of dielectric response

Citation: Piwowarczyk, M.; Juszyńska-Gałązka, E.; Gałązka, M. The Universal Scaling of Dielectric Response as a Tool in the Description of a Complex Dynamic of 4′-Butyl-4-(2-methylbutoxy)azoxybenzene (4ABO5*). *Crystals* **2024**, *14*, 95. https://doi.org/10.3390/cryst14010095

Academic Editors: Yanzi Gao, Cheng Zou, Meina Yu and Vladimir Chigrinov

Received: 21 December 2023
Revised: 15 January 2024
Accepted: 17 January 2024
Published: 20 January 2024

1. Introduction

Studies of the relaxation of any system, a phenomenon of the gradual return of a system to its equilibrium state after the removal of external disturbance, provide information about the dynamics of its elements and interactions between them. Broadband Dielectric Spectroscopy (BDS) allows one to obtain crucial information on the dielectric relaxation of systems with some disorders. In such systems, polar molecules show some degrees of reorientational freedom, as in the plastic–crystal phase or mesophases (smectic, nematic, and cholesteric phases), or of reorientational and translational degrees of freedom, as in the isotropic liquid phase. Then, one can measure complex dielectric permittivity ε^* as a function of the electric field frequency f ($\omega = 2\pi f$) and other (external) parameters such as temperature T, pressure p, external electric E, or magnetic H fields. For analyzing a large amount of experimental data, the Debye model (for example, see [1–3]) or phenomenological Debye-like stochastic models, such as Cole–Cole (CC) [1–4], Cole–Davidson (CD) [1–3,5,6], and Havriliak–Negami (HN) [1–3,7], are used, as given by the following complex equation:

$$\varepsilon^*(\omega) = \varepsilon_\infty + \frac{\Delta\varepsilon}{(1 + (i\tau\omega)^{1-\alpha})^\beta}, \quad (1)$$

where $\Delta\varepsilon$ is the dielectric increment, ε_∞ is the dielectric permittivity for the frequency tending to infinity, τ is the relaxation time, and α or β are exponents describing the symmetrical or asymmetrical distribution of relaxation time. The Debye model ($\alpha = 0$ and $\beta = 1$ in Equation (1)) describes the relaxation of the identical non-interacting electric dipoles in diluted systems. In contrast, the Debye-like models ($0 < \alpha < 1$ and $\beta = 1$ for the CC model; $\alpha = 0$ and $0 < \beta < 1$ for the CD model; and $0 < \alpha < 1$ and $0 < \beta(1 - \alpha) < 1$ for the HN model) describe the independently reorienting (non-interacting) electric dipoles in a viscous medium, which influence the distribution of relaxation times. In turn, the Dissado–Hill (DH) cluster model [8,9] describes the interacting electric dipoles, taking into account the exchange of energy between them as in real condensed phases, and it is given by Equation (2) as follows:

$$\varepsilon^*(\omega) = \varepsilon_\infty + \Delta\varepsilon(1 + i\tau\omega)^{-n}{}_2F_1(n, 1-m; 1+n; (1+i\tau\omega)^{-1})/{}_2F_1(n, 1-m; 1+n; 1), \quad (2)$$

where ${}_2F_1$ represents the Gaussian hypergeometric function [10]. The model proposed by Dissado and Hill is mathematically equivalent to the model proposed by Schönhals and Schlosser [11,12]. One can find that in all mentioned models and realms of dielectric (or electric) materials, the asymptotic frequency dependences of real and imaginary parts of complex dielectric permittivity are described by the power laws. In general, one can write that for low frequencies, i.e., $f \to 0$ ($\omega \to 0$), the power law is characterized by the exponent M $\varepsilon''(\omega)|_{\omega \to 0} \propto \omega^M$ and $(\varepsilon'(\omega) - \varepsilon_\infty)|_{\omega \to 0} \approx \Delta\varepsilon \propto \omega^{M=0}$, and for high frequencies, i.e., $f \to \infty$ ($\omega \to \infty$), the power law is characterized by the exponent N $\varepsilon''(\omega)|_{\omega \to \infty} \propto \omega^{-N}$ and $(\varepsilon'(\omega) - \varepsilon_\infty)|_{\omega \to \infty} \propto \omega^{-N}$ (for more details, see for example [13]), which agrees well with Jonscher's universal behavior [14]. The exponents M and N can be easily found for the mentioned models, i.e., $M = m = (1 - \alpha)$ and $N = n = \beta(1 - \alpha)$. Moreover, these exponents can be treated as measures of long-range and short-range (local) correlations of the molecular motions, respectively. The DH cluster model gives the exact values of the long-range and short-range correlation coefficients equaling $(1 - m)$ and $(1 - n)$, respectively. For the Debye-like models, one can obtain the approximated values of these coefficients—it is α for the long-range correlation and $(1 - \beta(1 - \alpha))$ for the short-range correlations.

To understand the dielectric response of any system and/or the impact of the long-range and short-range interactions on relaxation processes observed, some scaling procedures were proposed, such as by Nagel and co-workers [15–18] and references cited therein, by Dendzik and Paluch and co-workers [19], and by Gałązka and co-workers [13,20,21]. Proposed scaling procedures collapse numerous loss spectra (Nagel and Dendzik and Paluch scaling relations are restricted only to the imaginary part of ε^*, and Gałązka's scaling relation can be applied to both real and imaginary parts of ε^*; for more details, see [13,20,21]) onto a single primary curve; for example, see [13,15–21] and references cited therein. The scaling proposed by Nagel and co-workers is highly restricted for some systems, i.e., $M = 1$ and the exponent N equaling to the reciprocal value of the full width at half maximum divided by the full width at half maximum of the Debye peak, in decades of frequency [13]. The scaling procedures proposed by Dendzik and Paluch and co-workers and by Gałązka and co-workers show that the long-range and short-range correlations strictly dominate the shapes of various relaxation processes. In other words, one can say that the low- and high-frequency power laws, arising from the long-range and short-range interactions, describe the behavior of real and imaginary parts of ε^* on the asymptotic limits of frequencies, but their combination is valid in the vicinity of the maximum of ε'' or of the inflection point of ε'. Moreover, the scaling procedures can be used to characterize the relaxation processes observed. Two parameters of the scaling procedures are the exponents M and N, and some others are proportional to the relaxation time τ and the dielectric strength $\Delta\varepsilon$.

In describing molecular dynamics, it is important to accurately describe the relaxation response of the system. In the case of overlapping relaxation processes (for example, see [22–24]), i.e., for relaxation processes closely located and showing one peak of ε'' as the function of frequency f, it is almost impossible to separate such processes. Then, the method allows one to check (determine) whether at least two (or more) relaxation process overlaps are needed. Suppose the scaling of the dielectric response is not fulfilled. In that case, it indicates that one is dealing with at least two combined relaxation processes visible in the frequency dependence of ε'' as the single peak. This additional advantage of using dielectric response scaling will be demonstrated in the example of a cholesteric liquid crystal 4′-butyl-4-(2-methylbutoxy)azoxybenzene, abbreviated as 4ABO5* [25–27]. The use of a method that allows for a simple examination of the complexity of the relaxation process (i.e., the overlap of relaxation processes) is very important in the description of molecular dynamics. Although the dielectric response scaling method does not explicitly describe molecular dynamics (i.e., both the relaxation time and the dielectric increment are proportional to the parameters used in scaling), obtaining discrepancies in the scaled relaxation spectra allows one to draw conclusions about the complexity of these spectra from several (e.g., two) relaxation processes. Moreover, the greater the divergence from

the common scaled curve, the more distant "the components" of the (observed) relaxation process should be expected. This advantage of the dielectric response scaling will be described in detail.

The incomplete overlap of relaxation processes, e.g., around the short and the long axes of the molecule, resulting in a peak with two maxima or one distinct maximum and a "saddle" on one of the wings, most often occurs in liquid-like phases [22]. However, in the case of the coexistence of isomers in the sample, the overlap of relaxation processes may be complete (i.e., a single peak is observed for the imaginary part of the dielectric permittivity). This effect, if it occurs, can best be observed in the crystal phase, where the molecules have fewer degrees of freedom than in liquid-like phases or mesophases. Therefore, we used the crystal phase of 4ABO5* to show the power of the dielectric response scaling.

The liquid crystal 4ABO5* belongs to the homolog series of azoxybenzenes and azobenzene derivatives. In the literature, dialkyloazoxybenzenes are mostly abbreviated as *n*OAOB [28–30] and references cited therein for n = 1–14, where n stands for the number of carbon atoms in the symmetrical alkyloxy chains, or the dialkylazoxybenzenes, mostly abbreviated as *n*AOB [28,29,31,32], for n = 1–14, are described. The liquid crystal 7AOB is also abbreviated as HAB [32]. The physicochemical properties, as well as the phase sequences, are much more poorly described for the asymmetric azoxybenzene compounds, i.e., for derivatives for which the phenyl rings, connected via azoxy (-N(=O)=N-) or azo (-N=N-) groups, possess alkyl (or alkyloxy) chains with various numbers of carbon atoms, i.e., 10AB7 [33] (due to a nominal nomenclature, one can use the abbreviation 10AOB7 interchangeably), 4EOB (due to a nominal terminology, it can be abbreviated as 8AB2 or 8AOB2) [34], and 4ABO5* (it could also be abbreviated as 4AOBO5*) [25–27]. They can be abbreviated as *n*AOBO*m* or *n*AOB*m*, where n and m represent the number of carbon atoms in the alkyl chains. The phase transition temperatures and the number of thermodynamic phases observed depend on the lengths of the alkyl or alkyloxy chains; compare [25–33] for further information. The dielectric response of azoxybenzenes or azobenzenes is primarily described in the isotropic liquid phase (IL) or mesophases (i.e., liquid crystal phases)–nematic (N), cholesteric Ch (or chiral nematic N*) or smectics [25,28–32]. However, the relaxation processes in the crystal phase (Cr) are described for 4EOB [34], 10AB7 [33], and 4ABO5* (down to 250 K) [26,27] only. Thus, it is essential to describe the dielectric relaxation in the low temperatures of the crystal phase. The properties of 4ABO5* are described in [25] only for temperatures higher than 300 K (in the Ch and IL phases) and in [25–27] down to 250 K. Textures in the crystal phase from 250 K down to 200 K are almost the same. They are similar to the texture shown for T = 277 K in [26]. Only the brightness of the textures changes, which can be observed using the thermo-optical analyses, e.g., [35]. The negligible change in the intensity of light passing through the sample is connected with ordering the carbon atoms in the alkyl or alkyloxy chains. No additional transitions between crystal phases were noticed in BDS, differential scanning calorimetry, and polarized (light) optical microscopy techniques. 4ABO5* is a (weak) polar material [25–27].

We show that the scaling procedure is an excellent tool for checking the complexity (overlapping) of the relaxation processes. In addition, we describe the molecular dynamic of the chiral liquid crystal 4ABO5* in the crystal phase down to about 200 K.

2. Materials and Methods

The 4ABO5* substance was synthesized at the Military University of Technology, Warsaw (Poland), by the group of Prof. R. Dąbrowski.

The BDS measurements were carried out in two relaxation frequency ranges: 10^{-2} Hz to 40 MHz, called "the low-frequency range", and 1 MHz to 3 GHz, called "the high-frequency range". The samples were prepared in parallel plate geometry between two gold-plated electrodes with 20 mm or 7 mm diameters in the low- and high-frequency regions, respectively. The spaces between the electrodes were 100 µm and 220 µm, respectively. The dielectric permittivity was recorded in the low-frequency range using a high-precision

Novocontrol ALPHA analyzer, Montabaur, Germany. ZGS active sample cell test interface was used for the Alpha-A modular measurement system (Novocontrol), including the Pt100 temperature sensor. High-frequency RF measurements were carried out using a coaxial reflectometer based on the Agilent E4991 analyzer, Diegem, Belgium. The temperature was controlled by a Quatro Novocontrol cryo system with temperature stability of 0.1K in both experiments. More experimental details (i.e., the description of the sample preparation and experimental setup) are given in [26,36]. The high-precision Novocontrol ALPHA analyzer and the high-frequency Agilent E4991 analyzer are suitable for measuring the dielectric response of polar liquid crystals; for example, see [22,33,36–43].

3. Theoretical Background

To obtain a single scaled primary curve on which experimental data of $\varepsilon \equiv \varepsilon''(f)$ and/or $\varepsilon \equiv (\varepsilon'(f) - \varepsilon_\infty)$ are collapsed, the scaling relations in [13,20,21] have been proposed for abscissa (horizontal axis)

$$X \equiv \log\left(\frac{f}{f_s}\right) \tag{3}$$

and for the ordinate (vertical axis)

$$Y \equiv \frac{1}{M+N}\log\left(\frac{\varepsilon}{\varepsilon_s}\left(\frac{f_s}{f}\right)^{2M+N}\right), \tag{4}$$

where M and N are the exponents of power laws for the asymptotic frequencies, and f_s and ε_s are frequency and permittivity (real or imaginary parts) corresponding to the intersection of the power laws, respectively. Then, experimental data for various dielectric materials collapse onto the primary curve using Equations (3) and (4); for example, see [13,20,21]. In case one deals with complex spectra (i.e., overlapping relaxation processes), for example, two combined relaxation processes visible in frequency dependence of ε'' as the single peak, the scaling procedure will fail. This is because the scaling parameters obtained for the visible single relaxation process (composed of two closely located processes) do not accurately describe either long-range and short-range interactions or their combination.

Figure 1 shows examples of visible single relaxation processes (dashed curves) composed of two closely located relaxation processes (solid curves). The parameters of the individual processes are similar (i.e., $0.80 \le m \le 0.92$, $0.70 \le n \le 0.86$, $4{\cdot}10^{-6}\text{s} \le \tau \le 2{\cdot}10^{-5}\text{s}$) and the decimal logarithms, i.e., $\log(f_{max}/[Hz])$, of the distances between the position of the maximum of curve 1 and the positions of the maxima of curves 2, 3, 4, or 5 are 0.17, 0.29, 0.39, or 0.64, respectively. Tabulated data and the parameters of the individual processes (Equation (2)) can be found in the Supplementary Materials (file: 'Data_for_Fig1.txt'). Figure 2 presents the scaled complex curves of ε'' (combined of the two closely located curves shown in Figure 1). Tabulated data can be found in the Supplementary Materials (file: 'Data_for_Fig2.txt'). Scaled individual curves 1, 2, 3, 4, and 5 give one common primary curve (the solid red curve in Figure 2) with the maximal discrepancies on the kink not higher than 0.005. Such discrepancies are expected to appear on the scaled theoretical curves, and they are much higher than the adequate one obtained for scaled experimental processes; for more details, see [13,20,21]. However, the complex processes scaled using Equations (3) and (4) show higher discrepancies on the kink. The discrepancies between the scaled complex curves composed of two relaxation processes (*i*) 1 and 2; (*ii*) 1 and 3; (*iii*) 1 and 4; and (*iv*) 1 and 5 are about 0.005, 0.014, 0.036, and 0.092, respectively.

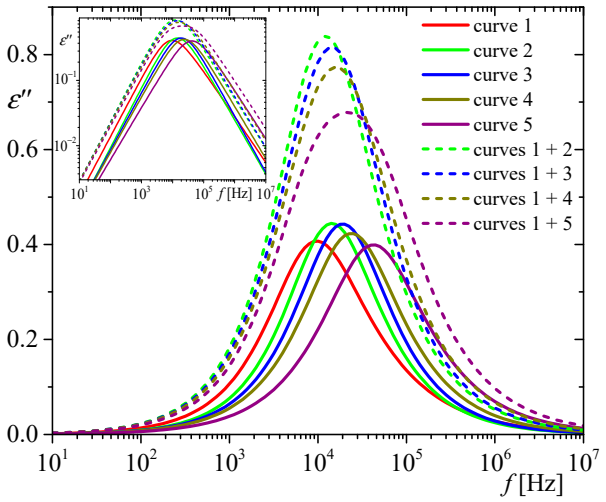

Figure 1. Theoretical curves of $\varepsilon''(f)$ (dashed curves) composed of two closely located relaxation processes (solid curves) obtained from the Dissado–Hill cluster model. Insert shows the dependences of $\varepsilon''(f)$ in log–log scales.

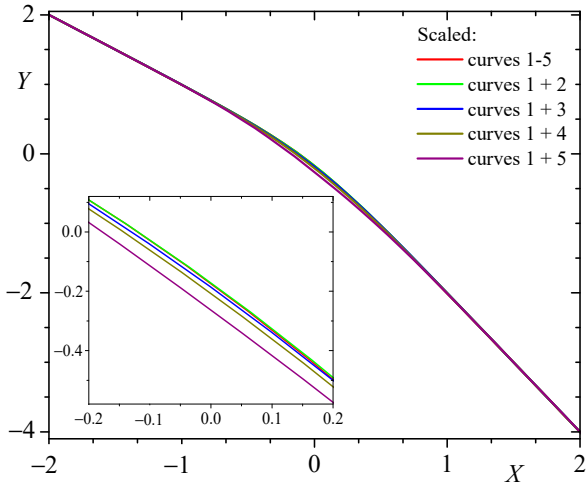

Figure 2. Scaled single curves of $\varepsilon''(f)$ (red curves) and curves composed of two relaxation processes (green, blue, dark yellow, and purple curves) with the use of scaling procedure given by Equations (3) and (4). Insert shows enlargement of the kink.

4. Discussion

The phase sequence in the cholesteric liquid crystal 4ABO5* is as follows: IL (298.82 K)–Ch (277.66 K)–Cr phases on cooling and Cr (285.26 K)–Ch (299.65 K)–IL phases on heating [26,27]. The Cr phase can be of the CONDIS type (conformationally disordered crystal phase) as the entropy changes in all phase transitions are insufficient to order functional groups in liquid crystal molecules [26,44–47]. Thus, some parts of the molecule may still have some degrees of freedom and can reorient in the Cr phase. In the CONDIS phase, molecules are transitionally (i.e., the centers of gravity of the molecules show translational order) and orientationally ordered, and the end chains show conformational changes (for example, see [44]).

BDS measurements show three relaxation processes [26]: (*i*) the low-frequency (or slow) relaxation process $\varepsilon''_{conf.}$ that can be ascribed to conformational motions of molecules privileged by interactions via the NO group; (*ii*) the medium-frequency relaxation process $\varepsilon''_{s.m.a.}$ ascribed to flip-flop rotation around the short molecular axis of molecules; and (*iii*) the high-frequency (or the fastest) relaxation process $\varepsilon''_{l.m.a.}$ ascribed to tumbling or rotation around the long molecular axis of molecules. The slowest relaxation process can be found

in the Ch and IL phases. It is hidden in either the conductivity region (ε'') or in the region of a contribution from the electrode polarization effect (ε'); for example, see [26]. The flip-flop relaxation was found in the IL, Ch, and Cr phases. The loss peak maximum is around 1 MHz in the IL phase, about 0.1 MHz in the Ch phase, and down to about 10 kHz in the Cr phase [26]. The fastest relaxation process, located around the long molecular axis or tumbling, was found in the IL, Ch, and Cr phases for frequencies higher than 1 MHz [26]. The frequencies for which the relaxation processes appeared are similar for other azoxybenzene or azobenzene derivatives [29–35] and references cited therein. The dominant relaxation process (i.e., with the highest dielectric increment) is the relaxation around the long molecular axis in the Ch and IL phases [26]. The relaxation around the short molecular axis becomes the dominant process in the low temperatures of the Cr phase, as compared with [26] and Figure 3c, whereas in the high temperatures of the Cr phase, the relaxation connected with the interactions via the NO group, $\varepsilon''_{conf.}$ or $\varepsilon'_{conf.}$, is the dominant process; for more, compare [26] and Figure 3a.

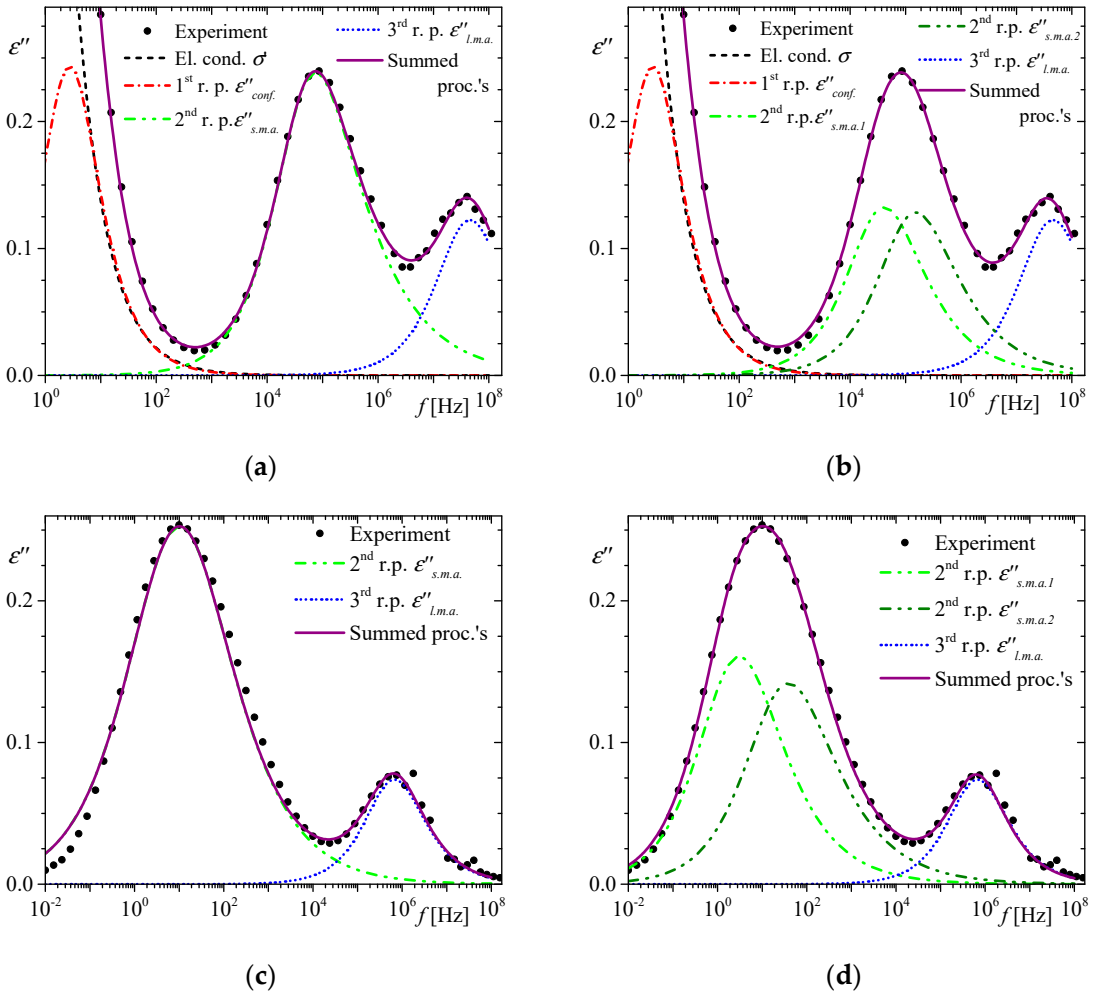

Figure 3. Experimental data (points) and theoretical fits, denoted as electric conductivity (dashed black curve), relaxation process ascribed to conformational changes (dash-dotted red curve), relaxation around the short molecular axis (dash-double dotted green and olive curves), relaxation around the long molecular axis (short dotted blue curve), and sum of all processes (thick purple curve) at selected temperatures of crystal phase: (**a**,**b**) at 275 K and (**c**,**d**) at 204 K. Figure (**b**,**d**) show fits for two relaxation processes around the short molecular axis.

Figure 3a,c show experimental data of $\varepsilon''(f)$ in the Cr phase and fits obtained for the two selected temperatures 275 K and 204 K, respectively. Fitting the HN functions, Equation (1), to the experimental data in the Cr phase, one finds that together with lowering

temperatures, the discrepancies between the experimental data and the fitted theoretical curves become more visible, especially for the relaxation around the short molecular axis. There is no possibility to obtain "perfect" agreement between experimental points and theoretical curves for the relaxation around the short molecular axis. Thus, we applied the scaling procedure, Equations (3) and (4), to the experimental data in the Cr phase to check the complexity (i.e., overlapping case) of the process observed. Figure 4 shows the scaled data for the selected temperatures for 4ABO5* and 4-ethyl-4'-octylazoxybenzene (4EOB). The 4EOB liquid crystal was chosen as a representative compound for scaling of the dielectric response. As has been shown, liquid crystals [13,20] and glass-forming compounds exhibiting hydrogen bonding or van der Waals bonding [13,20,21] are subject to dielectric response scaling. Tabulated experimental data presented in Figure 3a–d and the parameters of the HN equation, and scaled experimental data presented in Figure 4 can be found in the Supplementary Materials (file: 'Data_for_Fig3_experimental.txt', 'Data_for_Fig4_4ABO5st.txt' and 'Data_for_Fig4_4EOB.txt').

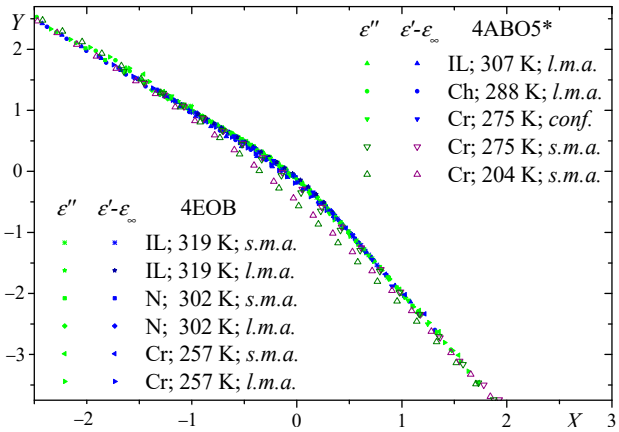

Figure 4. Scaled experimental data of $\varepsilon''(f)$ (green symbols) and $(\varepsilon'(f) - \varepsilon_\infty)$ (blue and purple symbols) for 4ABO5* and 4EOB liquid crystals at selected temperatures for various relaxations; *conf.*–ascribed to conformational changes, *l.m.a.*—around the long molecular axis, *s.m.a.*—around the short molecular axis, in different thermodynamic phases; IL—isotropic liquid, Ch—cholesteric (chiral nematic), N—nematic and Cr—crystal phases.

One sees that data scaled for IL, Ch, N, and Cr (for 4EOB and for $\varepsilon''_{conf.}$ and $\varepsilon'_{conf.}$ in 4ABO5*) lie on one common curve (filled symbols), whereas data scaled for $\varepsilon''_{s.m.a.}$, green open triangles, and $\varepsilon'_{s.m.a.}$, violet open triangles, at 204 K (up-triangles) and 275 K (down-triangles) in 4ABO5*, lie far away from the primary curve in the kink. The lower the temperature, the higher the discrepancy. It must be emphasized that to obtain the scaling parameters, one does not need to use any models. Thus, the discrepancies shown in Figure 4 are not a consequence of the "inexact" fits presented in Figure 3a,c. It just proves that one deals with two combined relaxation processes that are visible in the frequency dependence of ε'' as the single peak. The 4ABO5* is a mixture of isomers differing by location of the oxygen atom, which can be positioned to either of N atoms in the azo group [25]. The dipole moments of these isomers differ only slightly in [25] and references cited therein. Thus, one can expect to observe two relaxation processes located close to each other around the short molecular axes of the isomers. Separating such a complex peak into two component peaks is not unequivocal and simple. Moreover, several pairs of component peaks can be obtained. Because the origins of the relaxations for these isomers are the same, we assumed that the ratio of the dielectric strengths should be constant (or almost constant) in the whole temperature region. Figure 3b,d present the effect of such fits. One sees that the agreement between the experimental and theoretical curves is very good.

Figure 5 shows the relaxation times as a function of the inverse temperature in the Cr phase. Tabulated experimental data presented in Figure 5 can be found in the

Supplementary Materials (file: 'Data_for_Fig5.txt'). The half-filled green diamonds represent the values of $\tau_{s.m.a.}$ obtained for "inexact" fits of one HN function to the peak describing the relaxation around the short molecular axis, whereas the filled green and olive diamonds represent the values of $\tau_{s.m.a.1}$ and $\tau_{s.m.a.2}$, respectively, obtained for fits of two HN functions to the peak. The relaxation times are described by Arrhenius dependence [1–3], i.e., $\tau_{(i)} = \tau_0^{(i)} \exp(E_a^{(i)}/RT)$, where $E_a^{(i)}$ is the activation energy of the relaxation process (for $i = s.m.a.1$, $s.m.a.2$), and R is a gas constant. The activation energies are about 63.8 [kJ/mol] and 55.8 [kJ/mol] for $\tau_{s.m.a.1}$ and $\tau_{s.m.a.2}$, respectively. The activation energies for the rest relaxation processes, i.e., $\tau_{conf.}$ and $\tau_{l.m.a.}$, are about 87 [kJ/mol] and 10.7 [kJ/mol], respectively, and they coincide with the values reported in [26]. Obtained values of the activation energies are in agreement with the adequate ones reported for liquid crystals; for example, see [22,25,34,36,48–51]. The deconvolution of the relaxation process around the short axis of the molecule into two component processes, shown in Figure 3b,d, is only an example distribution. Such a process can be decomposed in several ways so that, while maintaining the assumed ratio of dielectric increment values at a similar level (i.e., about 1:1), several pairs of closely located relaxation processes can be obtained. They may differ in the location of the maxima, which affects the relaxation time τ. Moreover, they may show different dependences of the position of the maximum as a function of temperature, which affects the value of the calculated activation energy $E_a^{(i)}$, for $i = 1$ or 2. Therefore, the relaxation time values shown in Figure 5 are orientational values with a possible shift of up to approximately 10%. This means that the obtained activation energy values should be treated as the upper and the lower limits of the activation energy of the relaxation process around the short axis of the molecule.

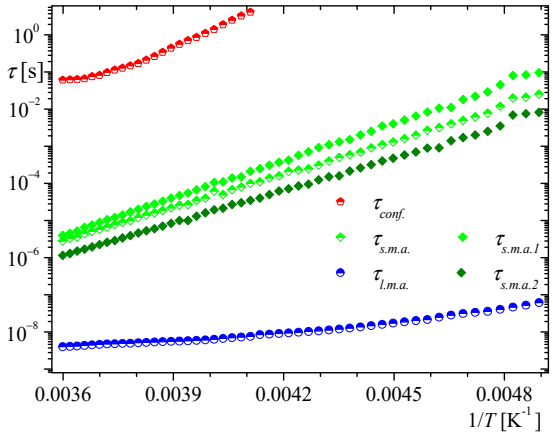

Figure 5. Dependences of the relaxation times for processes observed.

5. Conclusions

New insight into the behavior of chiral liquid crystal 4ABO5* in the broad temperature region in the Cr phase allows us to draw some main conclusions. There is no change in the behavior of $\tau_{s.m.a.1}$, $\tau_{s.m.a.2}$, and $\tau_{l.m.a.}$ for temperatures lower than 225 K. This temperature was expected to be the glass transition temperature, as reported in [26]. For the high temperatures of the Cr phase, the Vogel–Fulcher–Tammann (VFT) relation (for example, see [1,3,26]) can be fitted to the relaxation time $\tau_{conf.}$ as in [26]. However, the Arrhenius relation suits the experimental data for the low temperatures of the Cr phase. Similarly, as for the VFT relation, the Arrhenius relation states that the temperature for which the relaxation time is of the order of 100 s (the assumed value of the relaxation time for the vitrification process [1,3]) is about 226.5 K, which is consistent with the T_g published in [26]. But, no signatures of vitrification and softening of glass were detected in calorimetric and dielectric measurements around 225 K. Similar behavior was shown by other compounds from this homolog series, i.e., 4EOB [34] and 10AB7 [33]. The results suggest that the relaxation associated with the conformational motions of molecules or interactions via

the NO group becomes very weak. The dielectric increment is the decreasing function of decreasing temperature, and $\Delta\varepsilon_{conf.}$ takes values of about 0.43 at 277.8 K and 0.01 at 243.8 K.

The liquid crystal 4ABO5* is a mixture of isomers differing by location of the oxygen atom positioned to either of the azo group in proportion, almost, 1:1 ($\Delta\varepsilon_{s.m.a.1}/\Delta\varepsilon_{s.m.a.2} = 0.93 \div 0.97$). The relaxation process around the short axis of the molecule is composed of two processes located close to each other. The failure to satisfy the dielectric response scaling supports this hypothesis. Both processes are described by the HN equation with similar sets of exponents α and β, i.e., $\alpha_{s.m.a.1} \cong 0.3$, $0.75 \leq \beta_{s.m.a.1} \leq 0.80$ and $\alpha_{s.m.a.2} \cong 0.2.$, $\beta_{s.m.a.2} \cong 0.9$. Due to the fact that in the IL and Ch phases, the molecules have more degrees of freedom than in the Cr phase, these processes can be described by even more similar values of exponents and, what is important, is that the maxima of the loss peaks would coincide in IL and Ch phase. For compounds composed of two isomers, an overlapping relaxation process can occur around one of the molecule's axes in the crystal phase only. Relaxation around the short axis takes place at lower frequencies than relaxation around the long axis of the molecule (which is close to the upper limit of the measurement window, i.e., for frequencies higher than 1 MHz). Therefore, relaxation processes can be expected to overlap around the short axis of the molecule.

The scaling procedure proposed in [13,20,21] is an excellent tool for studying the complexity of molecular dynamics observed in dielectric materials. As shown, it allows one to check whether an observed relaxation process is a composition of several relaxational processes, as in the Cr phase of 4ABO5*. The more significant the difference in the scaled curves of the dielectric response (on the kink), the larger the separation of the maxima of possible component processes that should be expected.

Supplementary Materials: The following supporting information can be downloaded at https://www.mdpi.com/article/10.3390/cryst14010095/s1.

Author Contributions: Conceptualization, M.G.; methodology, M.G.; formal analysis, M.G.; investigation, M.G., M.P. and E.J.-G.; data curation, E.J.-G.; writing—original draft preparation, M.G.; writing—review and editing, M.G., M.P. and E.J.-G.; supervision, M.G. All authors have read and agreed to the published version of the manuscript.

Funding: This research received no external funding.

Data Availability Statement: The original contributions presented in the study are included in the article, further inquiries can be directed to the corresponding author.

Acknowledgments: We thank Andrzej Bąk from the Rzeszów University of Technology for help in dielectric measurements.

Conflicts of Interest: The authors declare no conflicts of interest.

References

1. Haase, W.; Wróbel, S. (Eds.) *Relaxation Phenomena*, 1st ed.; Springer: Berlin/Heidelberg, Germany, 2003.
2. Böttcher, C.J.F.; Bordewijk, P. *Theory of Dielectric Polarization*, 2nd ed.; Elsevier Science Publisher B.V.: Amsterdam, The Netherlands, 1979; Volume 2.
3. Kremer, F.; Schönhals, A. (Eds.) *Broadband Dielectric Spectroscopy*, 1st ed.; Springer: Berlin/Heidelberg, Germany, 2002.
4. Cole, K.S.; Cole, R.H. Dispersion and absorption in dielectrics I. Alternating current characteristics. *J. Chem. Phys.* **1941**, *9*, 341–351. [CrossRef]
5. Davidson, D.W.; Cole, R.H. Dielectric relaxation in glycerin. *J. Chem. Phys.* **1950**, *18*, 1417. [CrossRef]
6. Davidson, D.W.; Cole, R.H. Dielectric relaxation in glycerol, propylene glycol, and n-propanol. *J. Chem. Phys.* **1951**, *19*, 1484–1490. [CrossRef]
7. Havriliak, S.; Negami, S. A complex plane analysis of a-dispersions in some polymer systems. *J. Polym. Sci. Part C* **1966**, *14*, 99–117. [CrossRef]
8. Dissado, L.A.; Hill, R.M. A cluster approach to the structure of imperfect materials and their relaxation spectroscopy. *Proc. R. Soc. A* **1983**, *390*, 131–180. [CrossRef]
9. Dissado, L.A.; Hill, R.M. The fractal nature of the cluster model dielectric response functions. *J. Appl. Phys.* **1989**, *66*, 2511–2524. [CrossRef]

10. Oberhettinger, F. Hypergeometric functions. In *Handbook of Mathematical Functions with Formulas, Graphs, and Mathematical Tables*, 1st ed.; Abramowitz, M., Stegun, I.A., Eds.; National Bureau of Standards: Washington, DC, USA, 1964; Volume 55, pp. 555–566.
11. Schönhals, A.; Schloser, E. Dielectric relaxation in polymeric solids Part 1. A new model for the interpretation of the shape of the dielectric relaxation function. *Colloid Polym. Sci.* **1989**, *267*, 125–132. [CrossRef]
12. Schloser, E.; Schönhals, A. Dielectric relaxation in polymer solids Part 2: Application of the new model to polyurethane systems. *Colloid Polym. Sci.* **1989**, *267*, 133–138. [CrossRef]
13. Gałązka, M.; Juszyńska-Gałązka, E.; Osiecka, N.; Massalska-Arodź, M.; Bąk, A. On new scaling of dielectric response. *J. Appl. Phys.* **2015**, *118*, 064101. [CrossRef]
14. Jonscher, A.K. The 'universal' dielectric response. *Nature* **1977**, *267*, 673–679. [CrossRef]
15. Dixon, P.K.; Wu, L.; Nagel, S.R.; Williams, B.D.; Carini, J.P. Scaling in the relaxation of supercooled liquids. *Phys. Rev. Lett.* **1990**, *65*, 1108–1111. [CrossRef] [PubMed]
16. Menon, N.; Nagel, S.R. Comment on "Scaling of the α relaxation in low-molecular-weight glass-forming liquids and polymers". *Phys. Rev. Lett.* **1993**, *71*, 4095. [CrossRef] [PubMed]
17. Menon, N.; Nagel, S.R. Evidence for a divergent susceptibility at the glass transition. *Phys. Rev. Lett.* **1995**, *74*, 1230–1233. [CrossRef] [PubMed]
18. Dixon, P.K. Specific-heat spectroscopy and dielectric susceptibility measurements of salol at the glass transition. *Phys. Rev. B* **1990**, *42*, 8179–8186. [CrossRef] [PubMed]
19. Dendzik, Z.; Paluch, M.; Gburski, Z.; Zioło, J. On the universal scaling of the dielectric relaxation in dense media. *J. Phys. Condens. Matter* **1997**, *9*, L339–L346. [CrossRef]
20. Gałązka, M.; Juszyńska-Gałązka, E.; Osiecka, N.; Bąk, A. Universal scaling of dielectric response of various liquid crystals and glass-forming liquids. *Phase Trans.* **2016**, *89*, 341–348. [CrossRef]
21. Gałązka, M. Scaling of dielectric response of supercooled disordered phases. *Phase Trans.* **2018**, *91*, 231–238. [CrossRef]
22. Bąk, A.; Chłędowska, K. Role of surface interactions in the dynamics of chiral isopentylcyanobiphenyl mixed with Al_2O_3 powder as studied by dielectric spectroscopy: Numerical analysis. *Phys. Rev. E* **2011**, *83*, 061708. [CrossRef]
23. Tang, R.; Jiang, R.; Qian, W.; Jian, J.; Zhang, X.; Wang, H.; Yang, H. Dielectric relaxation, resonance and scaling behaviors in $Sr_3Co_2Fe_{24}O_{41}$ hexaferrite. *Sci. Rep.* **2015**, *5*, 13645. [CrossRef]
24. Buchner, R. What can be learnt from dielectric relaxation spectroscopy about ion solvation and association? *Pure Appl. Chem.* **2008**, *80*, 1239–1252. [CrossRef]
25. Roy, D.; Fragiadakis, D.; Roland, C.M.; Dąbrowski, R.; Dziaduszek, J.; Urban, S. Phase behavior and dynamics of a cholesteric liquid crystal. *J. Chem. Phys.* **2014**, *140*, 074502. [CrossRef] [PubMed]
26. Juszyńska-Gałązka, E.; Gałązka, M.; Massalska-Arodź, M.; Bąk, A.; Chłędowska, K.; Tomczyk, W. Phase behavior and dynamics of the liquid crystal 4'-butyl-4-(2-methylbutoxy)azoxybenzene (4ABO5*). *J. Phys. Chem. B* **2014**, *118*, 14982–14989. [CrossRef] [PubMed]
27. Gałązka, M.; Osiecka-Drewniak, N. Electric conductivity and electrode polarization as markers of phase transitions. *Crystals* **2022**, *12*, 1797. [CrossRef]
28. Urban, S.; Czub, J.; Gestblom, B. Comparison of dielectric properties of three alkyl and alkoxy azoxybenzenes (*n*AOBs and *n*OAOBs, *n* = 5, 6, 7) in the isotropic and liquid crystalline phases. *Z. Naturforsch. A* **2004**, *59*, 674–682. [CrossRef]
29. Domenici, V.; Czub, J.; Geppi, M.; Gestblom, B.; Urban, S.; Veracini, C.A. Dynamics of 4,4′-di-n-heptylazoxybenzene (HAB) studied using dielectric and ^{2}H NMR relaxation measurements. *Liq. Cryst.* **2004**, *31*, 91–99. [CrossRef]
30. Oka, A.; Sinha, G.; Glorieux, C.; Thoen, J. Broadband dielectric studies of weakly polar and non-polar liquid crystals. *Liq. Cryst.* **2004**, *31*, 31–38. [CrossRef]
31. Das, P.; Biswas, A.N.; Choudhury, A.; Bandyopadhyay, P.; Haldar, S.; Mandal, P.K.; Upreti, S. Novel synthetic route to liquid crystalline 4,4′-bis(n-alkoxy)azoxybenzenes: Spectral characterisation, mesogenic behaviour and crystal structure of two new members. *Liq. Cryst.* **2008**, *35*, 541–548. [CrossRef]
32. Kubo, K.; Matsumoto, T.; Mori, A.; Takahashi, H.; Takechi, H. Bis(4-dodecyloxyphenyl)diazene oxide. *Acta Cryst. E* **2005**, *61*, o3056–o3058. [CrossRef]
33. Drzewicz, A.; Moczkodan, Ł.; Juszyńska-Gałązka, E.; Jasiurkowska-Delaporte, M.; Deptuch, A. Phase behaviour and relaxation dynamics of the asymmetric azoxybenzene. *Phase Trans.* **2023**, *96*, 126–138. [CrossRef]
34. Gałązka, M.; Juszyńska-Gałązka, E.; Bąk, A.; Tomczyk, W. Phase behavior and dynamics of the liquid crystal 4-ethyl-4′-octylazoxybenzene (4EOB). *Phase Trans.* **2019**, *92*, 1089–1101. [CrossRef]
35. Osiecka, N.; Galewski, Z.; Massalska-Arodź, M. TOApy program for the thermooptical analysis of phase transitions. *Thermochim. Acta* **2017**, *655*, 106–111. [CrossRef]
36. Bąk, A.; Chłędowska, K.; Szaj, W. Role of the surface interactions in dynamics of 5*CB molecules in mixture with Al_2O_3 grains as studied by dielectric spectroscopy: Experimental results. *Mol. Cryst. Liq. Cryst.* **2010**, *533*, 82–91. [CrossRef]
37. Urban, S.; Lalik, S.; Różycka, A.; Iwan, A.; Marzec, M. Dielectric studies in the isotropic phase of six symmetrical azomethines with various number of benzene rings. Influence of the ionic conductivity. *J. Mol. Liq.* **2021**, *328*, 115477. [CrossRef]
38. Deptuch, A.; Jasiurkowska-Delaporte, M.; Urbańska, M.; Baran, S. Kinetics of cold crystallization in two liquid crystalline fluorinated homologues exhibiting the vitrified smectic C_A* phase. *J. Mol. Liq. A* **2022**, *368*, 120612. [CrossRef]

39. Deptuch, A.; Jaworska-Gołąb, T.; Dziurka, M.; Hooper, J.; Srebro-Hooper, M.; Urbańska, M.; Tykarska, M.; Marzec, M. Determination of tilt angle and its behavior in chiral smectic phases by exploring molecular conformations using complementary methods. *Phys. Rev. E* **2023**, *107*, 034703. [CrossRef] [PubMed]
40. Lalik, S.; Deptuch, A.; Fryń, P.; Jaworska–Gołąb, T.; Dardas, D.; Pociecha, D.; Urbańska, M.; Tykarska, M.; Marzec, M. Systematic study of the chiral smectic phases of a fluorinated compound. *Liq. Cryst.* **2019**, *46*, 2256–2268. [CrossRef]
41. Osiecka, N.; Massalska-Arodź, M.; Galewski, Z.; Chłędowska, K.; Bąk, A. Effect of flip-flop motion on dielectric spectra of highly ordered liquid crystals. *Phys. Rev. E* **2015**, *92*, 052503. [CrossRef]
42. Kolek, Ł.; Jasiurkowska-Delaporte, M.; Massalska-Arodź, M.; Szaj, W.; Rozwadowski, T. Mesomorphic and dynamic properties of 3F5BFBiHex antiferroelectric liquid crystal as reflected by polarized optical microscopy, differential scanning calorimetry and broadband dielectric spectroscopy. *J. Mol. Liq.* **2020**, *320*, 114338. [CrossRef]
43. Rozwadowski, T.; Jasiurkowska-Delaporte, M.; Massalska-Arodź, M.; Yamamura, Y.; Saito, K. Designing the disorder: The kinetics of nonisothermal crystallization of the orientationally disordered crystalline phase in a nematic mesogen. *Phys. Chem. Chem. Phys.* **2020**, *22*, 24236–24248. [CrossRef]
44. Wunderlich, B. A classification of molecules, phases, and transitions as recognized by thermal analysis. *Thermochim. Acta* **1999**, *340–341*, 37–52. [CrossRef]
45. Horiuchi, K.; Yamamura, Y.; Pełka, R.; Sumita, M.; Yasuzuka, S.; Massalska-Arodź, M.; Saito, K. Entropic contribution of flexible terminals to mesophase formation revealed by thermodynamic analysis of 4-alkyl-4′-isothiocyanatobiphenyl (nTCB). *J. Phys. Chem. B* **2010**, *114*, 4870–4875. [CrossRef]
46. Yamamura, Y.; Adachi, T.; Miyazawa, T.; Horiuchi, K.; Sumita, M.; Massalska-Arodź, M.; Urban, S.; Saito, K. Calorimetric and spectroscopic evidence of chain-melting in smectic E and smectic A phases of 4-alkyl-4′-isothiocyanatobiphenyl (nTCB). *J. Phys. Chem. B* **2012**, *116*, 9255–9260. [CrossRef] [PubMed]
47. Drzewicz, A. *Insight into Phase Situation and Kinetics of Cold- and Melt Crystallization Processes of Chiral Smectogenic Liquid Crystals*; IFJ PAN: Kraków, Poland, 2023. [CrossRef]
48. Rozwadowski, T.; Massalska-Arodź, M.; Kolek, Ł.; Grzybowska, K.; Bąk, A.; Chłędowska, K. Kinetics of cold crystallization of 4-cyano-3-fluorophenyl-4-butylbenzoate (4CFPB) glass forming liquid crystal. I. Nonisothermal process as studied by microscopic, calorimetric, and dielectric methods. *Cryst. Growth Des.* **2015**, *15*, 2891–2900. [CrossRef]
49. Stepanova, T.P.; Bursian, A.É.; Denisov, V.M. Dipole moment and mobility of molecules in nematic liquid crystals of the 4-n-butyl ester of [4′-n-hexyloxyphenyl] benzoic acid in the absence of external orienting fields. *Phys. Solid State* **2002**, *44*, 1993–2000. [CrossRef]
50. Kolek, Ł.; Massalska-Arodź, M.; Adrjanowicz, K.; Rozwadowski, T.; Dychtoń, K.; Drajewicz, M.; Kula, P. Molecular dynamics and cold crystallization process in a liquid-crystalline substance with para-, ferro- and antiferro-electric phases as studied by dielectric spectroscopy and scanning calorimetry. *J. Mol. Liq.* **2020**, *297*, 111913. [CrossRef]
51. Pawlus, S.; Mierzwa, M.; Paluch, M.; Rzoska, S.J.; Roland, C.M. Dielectric and mechanical relaxation in isooctylcyanobiphenyl (8*OCB). *J. Phys. Condens. Matter* **2010**, *22*, 235101. [CrossRef]